**Article:**

**PAPER • OPEN ACCESS**

# A remotely foldable and actuatable kinematic origami gripper

To cite this article: Miyako Mizuna *et al* 2025 *Smart Mater. Struct.* **34** 075031

View the article online for updates and enhancements.

# A remotely foldable and actuatable kinematic origami gripper

**Miyako Mizuna**[1,5]**, Xiao Chen**[2,5] (iD)**, Eiji Iwase**[1,3] **and Shuhei Miyashita**[2,4,*] (iD)

[1] Department of Applied Mechanics and Aerospace Engineering, School of Fundamental Science and Engineering, Waseda University, Tokyo, Japan
[2] School or Electrical and Electronic Engineering, The University of Sheffield, Sheffield, United Kingdom
[3] Kagami Memorial Research Institute for Materials Science and Technology, Waseda University, Tokyo, Japan
[4] Indigneo Institute for *in silico* Medicine, University of Sheffield, Sheffield, United Kingdom

E-mail: shuhei.miyashita@sheffield.ac.uk

CrossMark

## Abstract

The origami-inspired method of fabricating a 3D structure from a 2D sheet through folding offers significant advantages over conventional approaches, such as assembling, particularly in terms of speed, versatility, and the ability to function untethered. Compared to conventional structures composed of links and joints, crease-based hinges experience less friction, making them better suited for shape transformation and kinematic applications, particularly at smaller scales. In recent years, advancements in wireless self-folding technologies for smart sheet materials have led to growing interest in applications such as remotely creating precise structures and tools for use in hard-to-reach places, including inside the body. In this work, we introduce a novel origami gripper system that integrates a versatile crease design and a dual-stage magnetic actuation method. It allows a planar object to be wirelessly self-folded into a gripper, seamlessly enabling it to remotely grasp an object after formation. The gripper's novel crease design, inspired by scissors linkage systems, allows for sharper fold angles to achieve gripping behavior. The resulting gripper measures $48.75 \times 45 \, \text{mm}^2$ and weighs just $2.562 \, \text{g}$. Self-folding is driven by Joule heating induced by an external magnetic field, which contracts a heat-responsive shrink film at the hinges. A kinematic model describing the structure's transformation is presented alongside its physical implementation and proof-of-concept experimental verification, demonstrating the system's potential for untethered, programmable manipulation.

Supplementary material for this article is available online

Keywords: magnetic induction heating, self-folding, shape memory polymers, origami, origami gripper

---

## 1. Introduction

The realization of smart materials with physical programmable properties has been actively studied in recent years. Some of the smart materials exhibit kinematic characteristics of shape transformability, often realized as a joined-link mechanism produced by 3D printers [1–4]. However, when designing transformable structures at centimeter to millimeter scales, due to the accuracy of fabrication processes, the friction around structure joints becomes non-negligible thus hindering the expected motion.

In contrast, origami-inspired fabrication offers a transformative approach to creating 3D structures by folding 2D sheet materials. This method minimizes friction at hinges, enabling smooth and reliable transformations. By integrating active materials at hinge joints, a technique known as self-folding, these structures achieve programmable transformation while retaining the functional advantages of traditional linkage systems, such as precise shape and movement control. The resulting geometries and motion patterns can be accurately modeled through crease pattern design, allowing for tailored mechanical behavior [5, 6]. Additionally, origami structures provide exceptional versatility; by modifying fold creases, they can be adapted to achieve diverse macroscopic forms, altered physical properties (e.g. light deflection and absorption [7], electromagnetic inductance [8]), and specialized functionalities such as grippers [9–14], pH-responsive chemical carriers [15], and deployable scissors-like systems [16].

Self-folding technique is a widely used method in the field of micro-robotics as a way to drive the transition of origami structures. There are many stimuli of self-folding, including but not limited to heat [17–20], light [21, 22], pH [15, 23], magnetic field [24–26], and stretch force [27], etc. Heat-driven method is one of the most common stimulation methods, which achieves self-folding by triggering the deformation of shape memory materials (shape memory polymer, SMP, [28–30] or shape memory alloy, SMA, [31–34]) around the hinge joints, causing them to fold along specific directions, and these materials act as joints to drive the adjacent structure to fold through the torque generated by the deformation. However, the heat-driven self-folding method applied to a small-scale structure often requires a global heating environment to activate the deformation of the smart material by heating the environment around the structure. Such a requirement constrained the method to achieve better performance in the workspace where the ambient temperature is limited.

In the case of SMA, it can be stimulated either by global heating or by applying an electric current. However, SMA-based origami structures typically require a connection to a power supply, which limits their ability to operate remotely. While some SMA origami structures have been developed by embedding wireless receiving circuits that convert energy from an alternating magnetic field into current to stimulate the SMA [33], the added size and weight of these receiver components remain significant constraints.

In our previous study [35], we proposed a miniature origami robot made of electrically conductive material and SMP, which is capable of remotely heat-stimuli self-folding by magnetic induction, and remote navigation by an external magnetic field. However, with the conductive material, the 2D sheet of the origami robot becomes rigid. When the material is used as the exoskeleton of the origami robot, the adjacent planes contact each other after folding, making the overall structure stiff and stable, which lacks the flexibility to be further transformed.

This paper proposes a novel crease pattern of origami gripper design inspired by scissors linkage system that transforms from a flat deployed state to a 3D cylindrical shape that can act as a gripper. The hinge joint of the gripper is made of shape memory polymers, allowing each hinge joint to experience little friction and enable remote folding through magnet induction. Following the self-folding process, the hinges retain a degree of flexibility, allowing further actuation under an external magnetic field. The shape transformation mechanics were modeled using a bar linkage kinematic model, providing a theoretical basis for the design. To verify the performance of the proposed crease pattern, we fabricated a gripper that has a size of $48.75 \times 45\,\mathrm{mm}^2$ in sheet state. By applying magnetic induction, the fabricated sheet can be self-folded into an untethered origami gripper, and then be actuated to achieve grasping by an external magnetic field. Compared to existing tendon-driven and pneumatic origami gripper designs [10, 14, 36], the proposed system offers the significant advantage of being fully untethered, eliminating the need for onboard electronics, cables, or external mechanical connections during operation.

In this work, we present three key contributions to the field of remotely actuated origami systems: first, we propose a novel origami crease pattern that enables a single 2D sheet to be transformed into multiple distinct 3D configurations, including a functional gripper, by tuning a single design parameter. This versatile crease design, inspired by scissors linkage mechanisms, allows for sharper fold angles and more compact folding behaviors compared to traditional crease patterns, expanding the design space for multifunctional origami devices. Second, we develop a kinematic model that quantitatively describes the transformation behavior of the single-unit origami structure, capturing the relationship between input folding angles, unit cell geometry, and overall structural deformation. This model provides predictive capabilities for optimizing design parameters and actuation inputs, offering a robust theoretical foundation for controlled folding behavior. Third, we demonstrate a dual-stage actuation system that integrates magnetic induction heating to trigger self-folding via a heat-responsive shrink film, followed by magnetic field-driven manipulation for object grasping. This combination of wireless actuation mechanisms enables untethered, programmable transformation and functional deployment, offering significant advantages in terms of energy delivery, control precision, and application versatility. Together, these contributions

establish a new platform for the design and actuation of multi-functional, remotely operated origami devices, with potential applications in soft robotics, deployable tools, and biomedical systems.

## 2. Methods

We arrange the method section as follows. In section 2.1, we present the design of the self-folding origami gripper structure and develop a kinematics model of the structure. In section 2.2, we present the induction heating-based self-folding method and the experiment setup. We also show the magnetic actuation method applied on folded structure in section 2.3. Finally, we outline the fabrication process of the proposed origami sheet.

### 2.1. The kinematic origami gripper

The design and transformation process of the proposed kinematic origami structure is illustrated in figure 1(a). It consists of multiple identical single units with mountain fold hinges, valley fold hinges, and through cuts. The different ranges of the diagonal angle $\alpha$, which is between mountain fold and valley fold, provide three different types of folding patterns—positive diagonal angle ($\alpha > 0$, figure 1(a)), zero diagonal angle ($\alpha = 0$, figure 1(b)), and negative diagonal angle ($\alpha < 0$, figure 1(c)). Each structure has the same dimensions in length and width and consists of the same number of single units.

When $\alpha = 0$ (figure 1(b)), the mountain fold hinges are parallel to the valley fold hinges. When the structure is folding, both mountain fold and valley fold provide parallel compression direction which is parallel to the horizontal plane, it is not able to generate an out-of-plane translation during the transformation process. This structure is similar to the scissors linkage structure in the conventional bar linkage system.

When the diagonal angle is with a value, the compression direction of the mountain fold hinges is different from the valley fold and not parallel to the horizontal plane. The deviation of the diagonal angle provides an out-of-plane translation. The positive and negative values of diagonal angles affect the structure translation direction differently. When the value of the diagonal angle is positive, the overall folding direction of the origami structure is in the same half-space as the folding direction of the valley fold within the structure. When the value of the diagonal angle is negative, the folding direction of the origami structure is in the opposite half-space to the folding direction of the valley fold within the structure.

Compared with the structure with $\alpha = 0$, both positive and negative diagonal angle structures obtain higher compression ratios due to the out-of-plane transformations. Due to the fact that the positive diagonal angle structure contracts a majority of its components inward during the compression process, the structure becomes more compact and achieves a higher contraction ratio. Furthermore, the negative diagonal angle structure experiences collision between adjacent structures during the early stage of compression, which prevents the structure from contracting to a fully compressed state in experiments. We therefore chose the positive diagonal angle structure for the origami gripper.

Figure 2(a) illustrates the sketch of a $3 \times 2$ origami crease pattern which consists of six identical single units arranged in three rows and two columns. The edge length of the T-shape panel connected to the diagonal edge is $L_1$, and the edge length of the half T-shape panel connected to the diagonal edge is $L_2$. The distance between these two edges is $W_2$, and the widths of these two edges and their corresponding panels are $W_1$ and $W_3$, respectively. Figures 2(b) and (c) are the folding results of a single unit with different viewing angles under the same $\theta_{\text{in}}$. $\theta_{\text{in}}$ is the angle between the T-shape panel and the horizontal plane observed from the plane perpendicular to the main hinge ($yz$-plane).

As shown in figure 2(d), the global folding angle, $\theta_{\text{out}}$, is the angle between the bisector prolongation of the angle formed by the longer edges of the adjacent half T-shape panels and the $z$-axis located in the center of the main hinge in $xz$-plane. Four points related to the gripper performance are shown in figure 2(d). The position vector of point $P_2$ and $P_3$ after rotated by $\theta_{\text{in}}$ from the plane state are expressed from figure 2(d) as below,

$$\overrightarrow{OP_2} = \begin{bmatrix} L_2 \cos\theta_{\text{in}} \\ \frac{W_3}{2} + W_2 \\ L_2 \sin\theta_{\text{in}} \end{bmatrix}, \tag{1}$$

$$\overrightarrow{OP_3} = \begin{bmatrix} (L_2 - W_2 \tan\alpha)\cos\theta_{\text{in}} \\ \frac{W_3}{2} \\ (L_2 - W_2 \tan\alpha)\sin\theta_{\text{in}} \end{bmatrix}. \tag{2}$$

In addition, vector $\overrightarrow{P_2P_1}$ forms an angle $\theta_{\text{in}}$ with the $z$-axis due to the linkage mechanism. The angle between the projection of $\overrightarrow{P_2P_1}$ onto the $yz$-plane and the $z$-axis is defined as $\theta_{\text{out}}$, as illustrated in figure 2(d). The vector $\overrightarrow{P_2P_1}$ can be expressed as follows:

$$\overrightarrow{P_2P_1} = \begin{bmatrix} -L_2 \cos\theta_{\text{in}} \\ -L_2 \sin\theta_{\text{in}} \sin\theta_{\text{out}} \\ L_2 \sin\theta_{\text{in}} \cos\theta_{\text{out}} \end{bmatrix}. \tag{3}$$

Based on the position vector of point $P_2$ and $\overrightarrow{P_2P_1}$, we derive the coordinates of point $P_1$ as:

$$\overrightarrow{OP_1} = \begin{bmatrix} 0 \\ \frac{W_3}{2} + W_2 - L_2 \sin\theta_{\text{in}} \sin\theta_{\text{out}} \\ L_2 \sin\theta_{\text{in}} (\cos\theta_{\text{out}} + 1) \end{bmatrix}. \tag{4}$$

With $\overrightarrow{OP_1}$ and $\overrightarrow{P_1P_4}$ located on the $yz$-plane at $x = 0$, we can further derive the coordinates of point $P_4$ as:

$$\overrightarrow{OP_4} = \begin{bmatrix} 0 \\ \frac{W_3}{2} + W_2 + W_1 \cos\theta_{\text{out}} - L_2 \sin\theta_{\text{in}} \sin\theta_{\text{out}} \\ L_2 \sin\theta_{\text{in}} (\cos\theta_{\text{out}} + 1) + W_1 \sin\theta_{\text{out}} \end{bmatrix}. \tag{5}$$
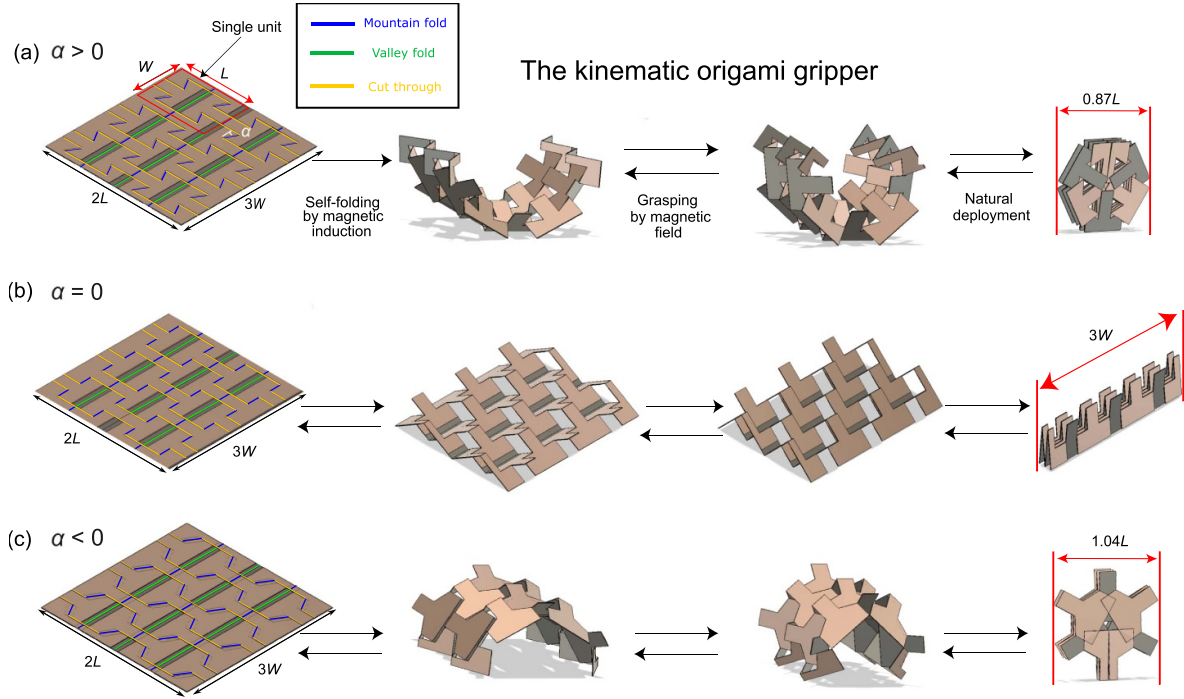
**Figure 1.** The deformation process of the origami structure with different diagonal angles. Kinematic origami gripper (positive diagonal angle) (a), scissors structure (diagonal angle = 0°) (b), and modified origami gripper (negative diagonal angle) (c).

Since the angle formed between vectors $\overrightarrow{P_2P_1}$ and $\overrightarrow{P_2P_3}$ is $90° - \alpha$, the global folding angle, $\theta_{out}$, can be determined as:

$$\theta_{out} = 2\arctan\left(\tan\alpha\sin\theta_{in}\right). \tag{6}$$

$P_1'$, is the point of $P_1$ symmetric about the $z$-axis. The distance $P_1$ and $P_1'$, $W_{out}$, can be calculated as:

$$W_{out} = 2\left(\frac{W_3}{2} + W_2 - L_2\sin\theta_{in}\sin\theta_{out}\right). \tag{7}$$

Here, $W_{out}$ represents the compression distance for a single unit. The radius, $r$, of a single folded unit is given by:

$$r = \frac{\frac{W_3}{2} + W_2 - L_2\sin\theta_{in}\sin\theta_{out}}{\sin\theta_{out}}. \tag{8}$$

Figure 2(e) illustrates a structure consisting of multiple units, we defined the folding angle of the multiple-unit structure as the global folding angle, $\phi_{out}$, which can be expressed:

$$\phi_{out} = 2N\theta_{out} = 4N\arctan\left(\tan\alpha\sin\theta_{in}\right), \tag{9}$$

where $N$ is the number of columns.

We conducted modeling calculations based on the equations above to analyze the deformation of the origami gripper (figure 3). Figure 3(a) shows the relationship between diagonal angle $\alpha$ and global folding angle $\theta_{out}$ with different main hinge folding angle $\theta_{in}$ ranging between 15° and 90°. When $\alpha > 0$, all $\theta_{out}$ are positive and $\theta_{out}$ gradually increased from 0° to 180°. In contrast, when $\alpha < 0$, all curves are symmetric with respect to the point in $\alpha = 0°$ compared to $\alpha > 0$. Figure 3(b) shows the trajectory of $P_1$ and $P_1'$ when $\theta_{in}$ is

changed from 0° to 90° with $\alpha = 30°$. The $z$-coordinates of two points are increased from 0 mm and reach the highest point through the origami structure deformation. The $x$-coordinate of both points close rapidly because two half T-shape panels next to the main T-shape panels in the center lean inside the structure as the side views of the structure in $\theta_{in} = 30°$ and 60°. The $x$-coordinate of the two points gradually changed to 0 mm and two curves intersect. Finally, the bottom of two half T-shapes comes over the center main T-shape to the opposite side. To see how $\alpha$ and $\theta_{in}$ affect the deformation, we put four plots of $\theta_{out}$ and $W_{out}$ with $\alpha = 30°$ and 45° by changing $\theta_{in}$ in figure 3(c). Compared to the result of modeling in $\alpha = 30°$ and 45°, $W_{out}$ with $\alpha = 30°$ is smaller than its with $\alpha = 45°$ before each plot reaches 0°. In addition, $\theta_{out}$ at $\alpha = 30°$ is smaller than its with $\alpha = 45°$. Therefore, by changing the diagonal angle $\alpha$, the deformations of the final structure are different, which enables the gripper to fit the object's dimension to grasp.

### 2.2. Self-folding by magnetic induction

The self-folding process of the origami structure is driven by magnetic induction heating. When the conductive material is placed into an alternating magnetic field, it generates a time-varying induced current, which generates joule heat with the resistance in electrical-conductive material. When the conductive material, copper in this study, is heated up to a certain temperature, it triggers the thermal response shape memory polymer (polyvinyl chloride—PVC is used in this paper) to shrink. Because the PVC sheet is sandwiched by the copper sheets using adhesive, it produces torque to drive the
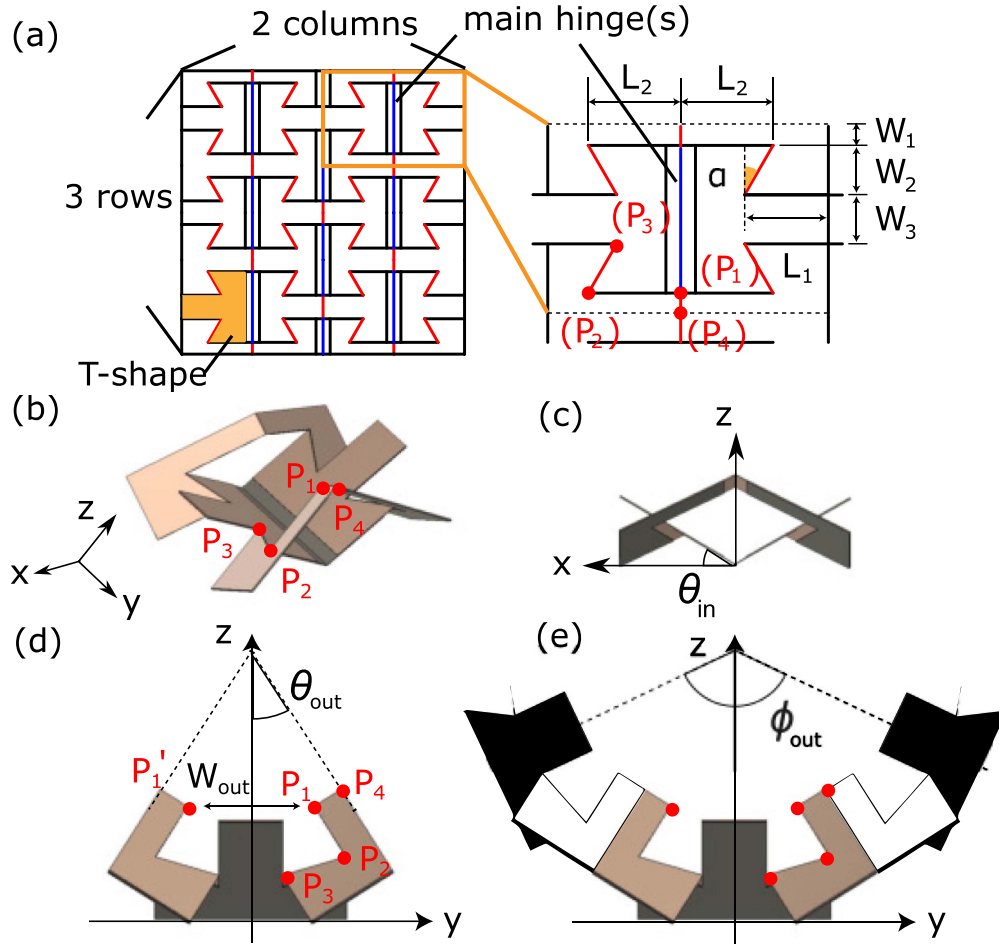
**Figure 2.** The net diagram and 3D deforming model at $\theta_{in} = 30°$. (a) The designed pattern (3 rows × 2 columns), parameters and points with parentheses which are going to be $P_1$, $P_2$, $P_3$ and $P_4$ (b) from bird view and (c)(d) from side view. Points $P_1$, $P_2$, $P_3$ and $P_4$, the distance $W_{out}$ and the global folding angle $\theta_{out}$ are shown in (d) for single unit. (e) Shows the several units and the total global folding angle, $\phi_{out}$.

copper layer to move during the shrinking process to achieve self-folding.

The temperature increase of the copper sheet over time $t$, $T(t)$, is given by [35]:

$$T(t) = \left(1 - e^{-\frac{\beta S}{\rho S d_r c_p}t}\right)\frac{P_{Joule}}{\beta S} + T_a, \quad (10)$$

where $S$ is the conductive surface area of the sample copper sheet, $\rho$ is the density of the sample ($8.96\,\text{g cm}^{-3}$), $d_r$ is the thickness of the test sample, $c_p$ is the specific heat capacity of the sample materials ($390\,\text{J kg K}^{-1}$ for copper), and $T_a$ is the room temperature during the experiment. The convective heat transfer coefficient, $\beta$, is given by solving the following equation:

$$\beta\left(T_d(t) - T_a\right) = -\rho d_r c_p \frac{dT_d(t)}{dt}, \quad (11)$$

where $T_d(t)$ is the cooling temperature of the sample sheet. A detailed model to predict the induction heating self-folding by considering factors such as the heat rates of the copper receivers, their design, materials, position on the coil, and magnetic field characteristics is described in [37].

### 2.3. Experiment setup and actuation

Figure 4 illustrates the experimental setup of the induction heating and actuating origami gripper. The system includes one horizontal induction coil for magnetic induction self-folding, and one horizontal actuation coil for grasping movements. The induction heating coil is placed 4 mm under the workspace surface and embedded into the center of the actuation coil.

The induction heating coil is wound outward from the center, with a diameter of 76 mm and a thickness of 5.8 mm. It is designed as a double-layer coil comprising 200 strands of enameled wire, manually braided into a Litz wire configuration. An alternating magnetic field with a resonant frequency of 100 kHz is applied to the coil.

The actuation of the origami gripper is controlled by a horizontal actuation coil located below the induction coil. 16 pieces of $2 \times 2 \times 2\,\text{mm}^3$ cubic neodymium magnets (N45) are attached to the back side of the origami sheet with their north pole facing upward. After the self-folding process is completed by the induction coil, the origami structure is then driven to open and close by a vertical magnetic field generated from the horizontal actuation coil.
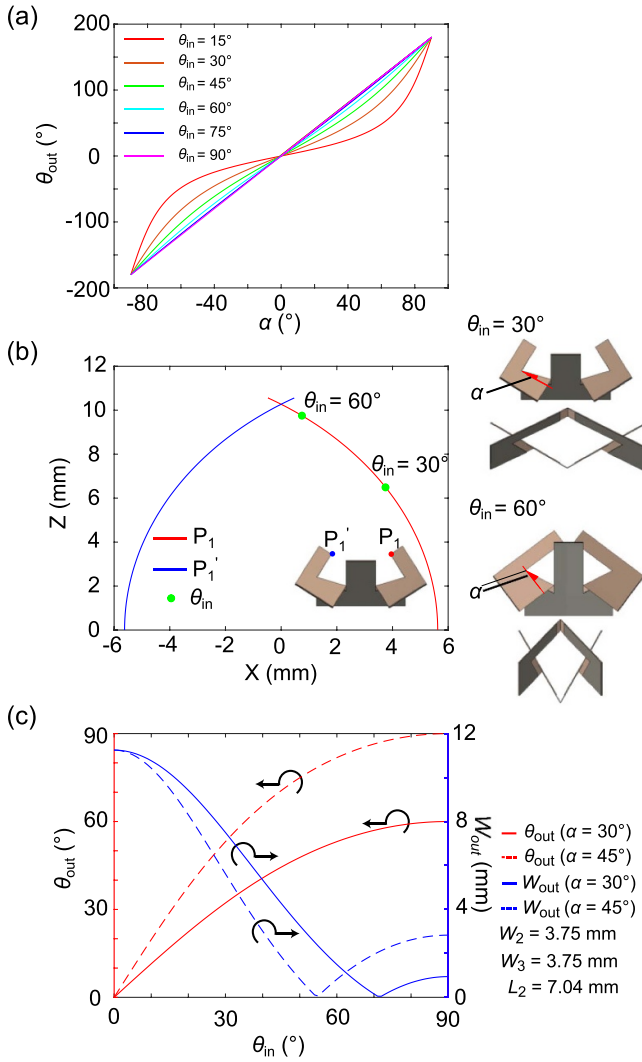
**Figure 3.** Simulation results of origami structures. (a) The relationship between diagonal angle $\alpha$ and $\theta_{out}$, (b) the locus of $P_1$ when $\alpha = 30°$, (c) the relationship between $\theta_{in}$, $\theta_{out}$ and $w_{out}$ when $\alpha = 30°$ and $\alpha = 45°$.

Figure 5 shows the final pattern of the origami gripper whose size is 45 mm in width and 48.75 mm in length. The V-shaped holes, which are located around the through cuts, are proposed to reduce the collision and friction between adjacent T-shape panels when deforming.

### 2.4. Fabrication

The origami gripper shown in figure 5 consists of three layers: the structural layers which are used copper ($50\,\mu$m thick) in this paper and a shape memory polymer contraction layer. Figure 6 illustrates the fabrication process of the self-folding sheet. The contraction layer, which is made of thermo-responsive PVC (24 $\mu$m thick) film, is sandwiched by two structural layers using heat-resistant silicone adhesives (High-Temperature Glue-on-a-Roll, McMaster-Carr, 20 $\mu$m thick). Two copper structural layers are cut by a vinyl cutter (Silhouette Cameo 3) into a design pattern with mountain

creases and valley creases. In the fabrication process, after one copper sheet placed on the mat was cut, place the silicone tape over that layer (figures 6(a)–(c)). Then, cut the silicon tape (figure 6(d)). Peel off the back layer which sandwich the PVC layer by two copper structural layers (figures 6(e) and (f)). Removing the external PVC (figure 6(g)), the origami part of the gripper is then ready to be attached with magnets using silicone tape.

## 3. Results

### 3.1. Induction induced self-folding of single-unit and multiple-unit structure

Figure 7 and supplementary video S1 shows the induction heating-based self-folding results of a $1 \times 1$ single-unit structure (figures 7(a)–(d)), a $2 \times 1$ multiple-unit structure (figures 7(e)–(h)) and a $3 \times 1$ multiple-unit structure (figures 7(i)–(l)). The unit in each origami was made in the same dimensions ($18.75$ mm $\times 22.5$ mm). All the structures were not attached with magnets. The figure shows as the number of single structural units increases, the overall folding angle increases. However, it also increases the weight and area of the structure, resulting in a decrease in heating efficiency. Therefore compared with the $1 \times 1$ unit structure and $2 \times 1$ multiple-unit structure, the heating time of the $3 \times 1$ multiple-unit structure increased. Figure 8 illustrates the comparison of the simulated global folding angle $\phi_{out}$ with the experimental results. The global folding angle of the origami structure and the main hinge folding angles were measured by the image tracking software (Tracker). All three sheets with different numbers of units were all stopped further folding when the main hinge folding angle, $\theta_{in}$, was around 60°. This may be because the area of the structure that is perpendicular to the magnetic field decreases as the folding angle increases, and the energy received is less than the heat loss of the environment when $\theta_{in}$ was around 60°, resulting in the hinges not able to be obtained more energy for shrinking.

In addition, the global folding angles of the three types of structures were smaller than the results of the simulation, this is because each diagonal hinge is only connected by PVC, which still has a certain folding ability in the direction perpendicular to the diagonal hinge. During the self-folding process, the structure was compressed in the perpendicular direction under the influence of gravity, which leads to the difference between the experimental results and the simulation results.

### 3.2. Magnetic grasping and releasing origami structure

The origami structure was placed on the center of the platform with magnets attached to the bottom layer. The horizontal coil generates a vertical magnetic field that has an opposite direction of the magnets, causing the structure with the magnets to start repelling and moving away from the plane. Figure 9 shows the relationship between the global folding angle $\phi_{out}$ and the applied magnetic flux density. The magnetic flux density was measured manually by a Gauss meter (Hirst GM07).
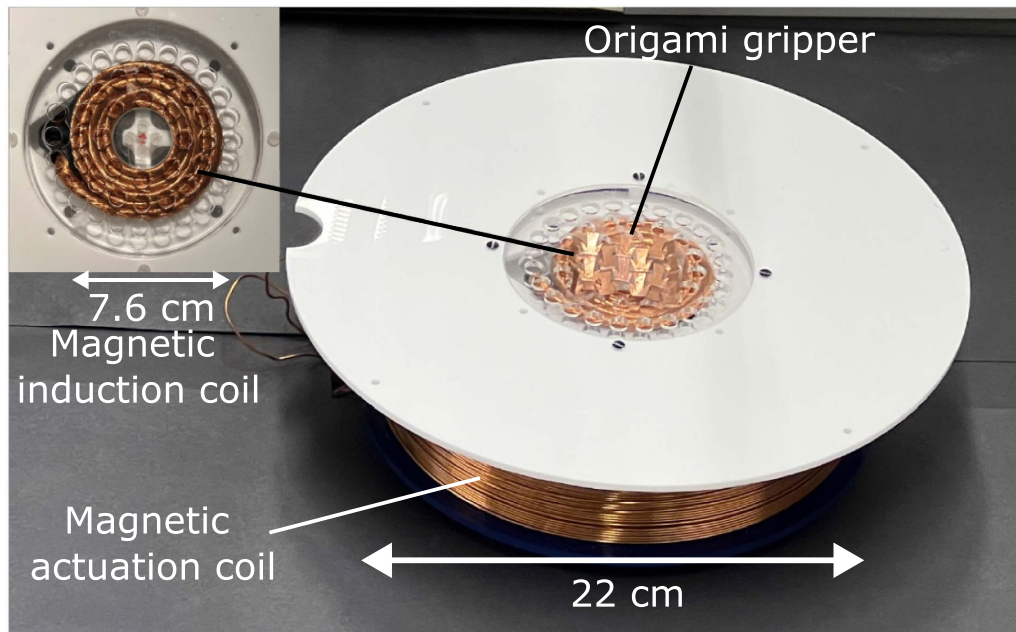
**Figure 4.** The experiment setup consisting of a magnetic induction coil, and a horizontal actuation coil.
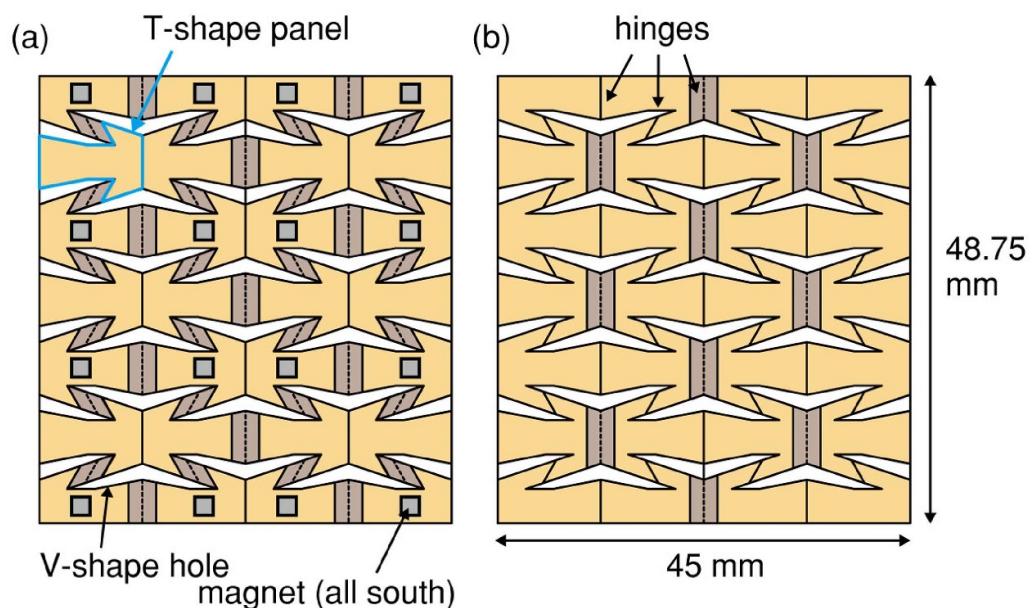


**Figure 5.** The final design of origami gripper. This design includes four areas: copper T-shape panel, hinges that drive folding due to PVC shrinkage, holes with no space and magnets. (a) Back layer, (b) front layer.

To evaluate the grasping performance of the structure actuated by the magnetic field, figure 10 shows the performance of the gripper grasping different objects and cotton in different sizes and weights. Each object was placed in the center of the platform and the origami gripper was held horizontally above the object by a pair of non-magnetic tweezers, with the folding direction facing downwards to minimize the influence of the structure's own weight on the experiment's performance. The magnetic flux density of the horizontal coil was incrementally increased, causing the origami

sheet to fold and securely hold the object. When the gripper was closed, it was lifted to see if the cotton was lifted together. Each cotton with different sizes and weights was tested five times, and the success rate was derived and shown in figure 10(b). A boundary curve, generated from the successful data points using MATLAB, outlines the region where the gripper achieved reliable performance (success rate >50%). All grasping experiments presented in this section were performed using the same gripper sample. No observable fatigue or mechanical degradation of the PVC
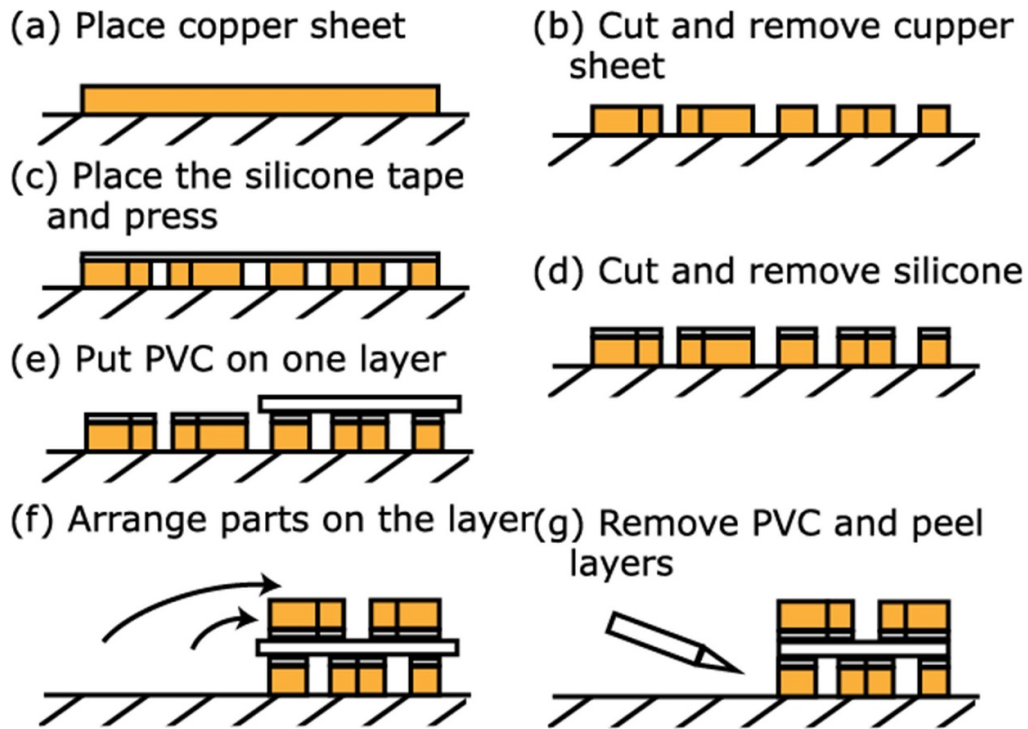
**Figure 6.** Origami sheet fabrication process, the sheet is cut by a vinyl cutter.
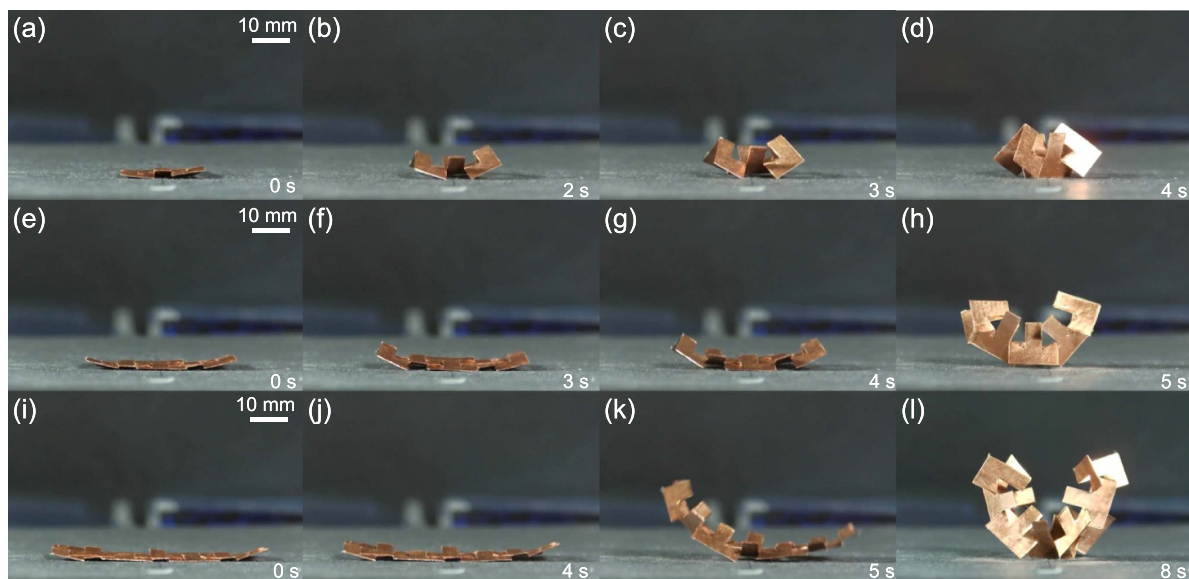


**Figure 7.** No magnets induction heating self-folding process with a single ($1 \times 1$) unit (a)–(d), $2 \times 1$ unit structure (e)–(h), and $3 \times 1$ unit structure (i)–(l). The full process is also shown in supplementary video S1.

hinges was detected after repeated grasping and releasing operations.

### 3.3. Seamlessly performance from self-folding and grasping

The experiment (figure 11 and supplementary video S2) shows the whole process of the origami structure self-folding by the magnetic induction coil and grasping a cotton swab by the magnetic actuation coil. 16 pieces of $2 \times 2 \times 2$ mm$^3$ sized

cubic magnets were attached to the origami sheet as described in section 2.3 after fabrication. The sheet was placed above the center of the magnetic induction coil. When the induction coil was on, the flat origami sheet was folded into a 3D structure. After the self-folding process was completed, the structure was actuated by the magnetic actuation coil. A strength-increasing magnetic field was generated by the actuation coil in the opposite direction of the magnets placed on the origami structure, causing the repulsive force on the magnets to drive
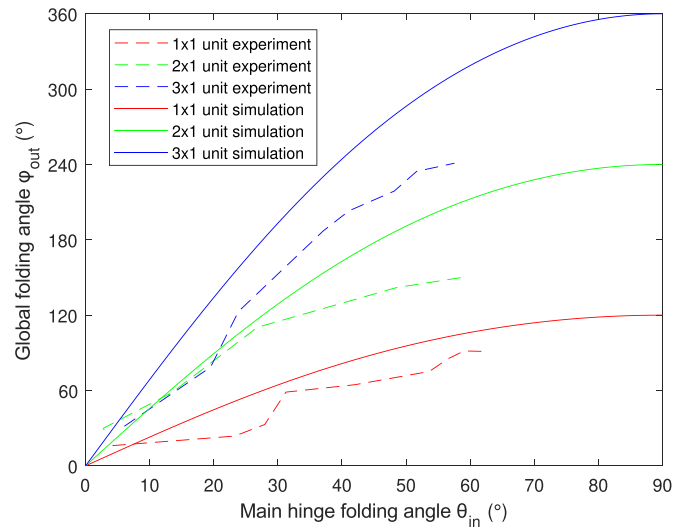
**Figure 8.** The global folding angles with different numbers of units. Each dash line expresses the experimental simulation result.
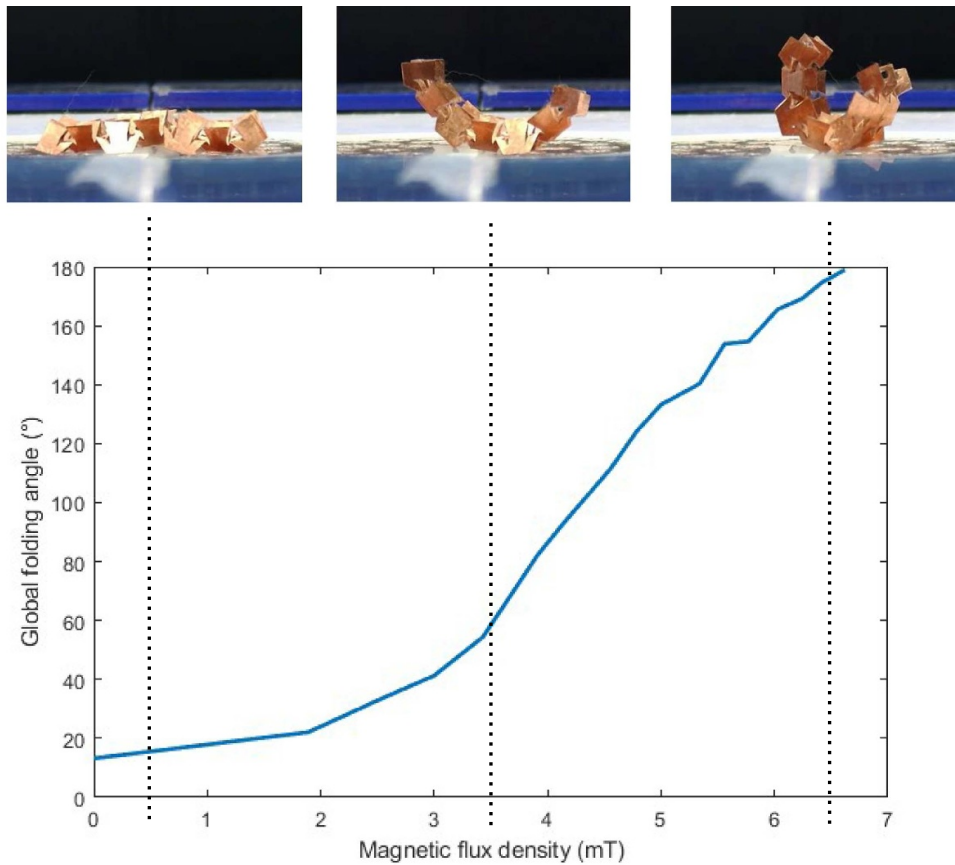


**Figure 9.** Relationship between global folding angle and applied magnetic flux density.

the whole structure away from the plane, leading the structure to fold further. During the application of the magnetic field, the gripper was able to grasp a cotton swab and overcome its own gravity to lift up when the cotton rose. When the actuation coil was turned off, the gripper released the cotton and it dropped to the platform.
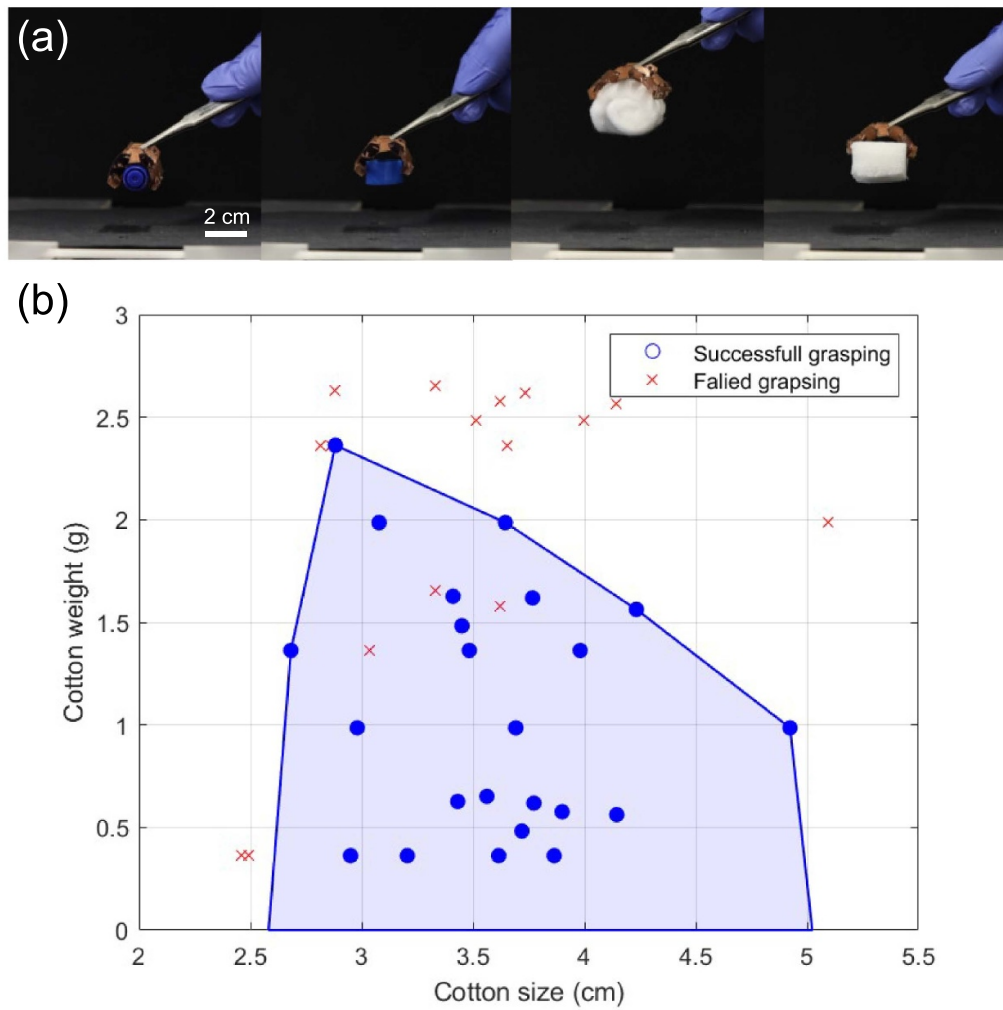
**Figure 10.** Grasping performance of the gripper with different objects undering an applied magnetic field. (a) Grasping results with different objects. (b) Grasping performance of cotton with different sizes and weights. The blue circle and the red cross indicate the successful grasping circle and the failed grasping cross. The blue field indicates the ideal success grasping region.
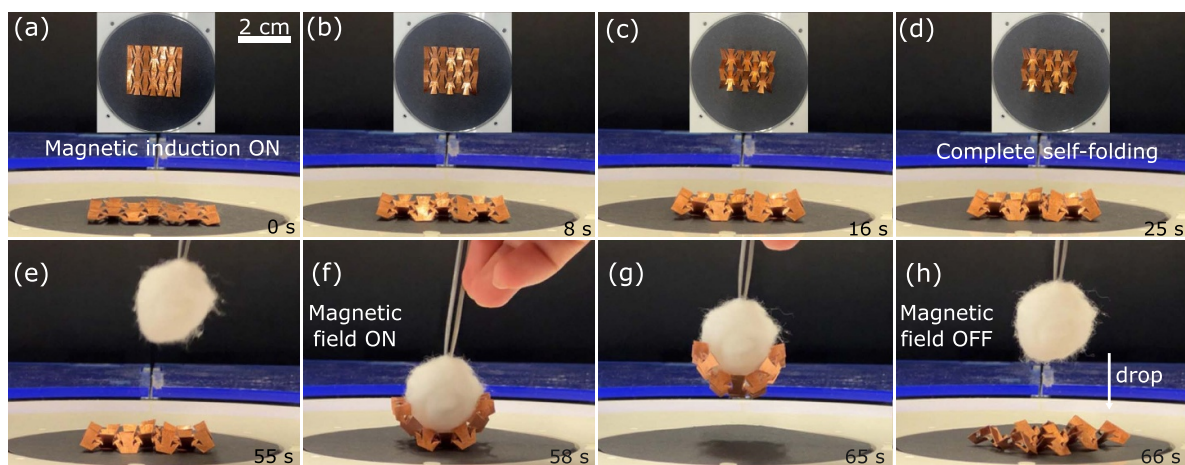


**Figure 11.** Magnetic induction induced self-folding, grasping of the origami gripper. (a) Placement of the origami sheet and turning on the magnetic induction coil. (b)–(d) Self-folding of the copper origami sheet. (e)–(h) Grasping performance of the self-folded origami gripper, with horizontal actuation coil on, the gripper starts grasping the cotton and can be lifted up will anchoring the cotton. The gripper will drop off when turning off the actuation coil. The full process is also shown in supplementary video S2.

The alignment of the cube magnets caused the structure pre-folded in advance of the heating process due to repulsive forces. It also prevented the situation where some hinges folded in the opposite direction to the expected direction due to the collision at the diagonal hinge during the self-folding process. However, the inclusion of magnets introduces additional weight to the structure, increasing its overall weight from 1.602 g to 2.562 g. The increased weight exceeded the torque capacity of the PVC at the hinge, rendering it insufficient to lift the adjacent copper structure as intended.

Furthermore, the orientation of the magnet placement serves to restrict the folding of the overall structure in the roll direction, which also results in a reduction in the overall compression rate of the structure. These combined factors—including increased structural weight, limited hinge torque generated by PVC, and restricted folding freedom— contribute to the relatively long deformation time observed in the experiments.

In addition, discrepancies were observed between the self-folding results and the model predictions. Each hinge is solely supported by PVC sheets, which limits the torque generated during self-folding. Consequently, if the structure's weight exceeds a certain threshold, the PVC cannot provide sufficient support to lift the structure out of the plane. Future improvements may include adding bridges between adjacent patterns (as in [18]) or implementing consecutive stilts along the hinge to enhance stiffness and structural integrity (e.g. [30]).

## 4. Conclusion

This study presents a remotely foldable and actuatable kinematic origami gripper inspired by the mechanical principles of scissors linkage systems. The gripper utilizes mountain and valley folds connected by shape memory polymer hinges, minimizing joint friction and enabling smooth self-folding and magnetic field-driven actuation for grasping tasks at sub-centimeter scales. The thermal stimuli required for self-folding are delivered via magnetic induction, which remotely heats the structural copper layer of the gripper. Additionally, a kinematic model of the system is developed and experimentally validated, providing a quantitative understanding of the gripper's folding and actuation mechanics. This integrated design shows promise for further miniaturization and potential applications as a remotely self-assembled functional structure.

Future work will focus on optimizing the origami fabrication process and system design to incorporate a larger number of unit cells within the same device footprint. This includes improving magnetic induction heating uniformity across larger-scale structures and balancing the trade-offs between added structural stiffness from inter-unit contact and the actuation energy required to achieve full folding. To ensure long-term operational reliability, systematic fatigue testing of the PVC hinge structures will be conducted, especially under repeated actuation cycles. Additionally, developing a coupled electromagnetic–thermal–mechanical model to quantitatively link the applied magnetic field strength to the resulting gripping force will provide valuable guidelines for optimizing actuation efficiency and performance. Exploring alternative material configurations and crease layouts may further enhance the scalability, versatility, and energy efficiency of the origami gripper system under different operating conditions.

## References

[1] Calì J, Calian D A, Amati C, Kleinberger R, Steed A, Kautz J and Weyrich T 2012 3D-printing of non-assembly, articulated models *ACM Trans. Graph.* **31** 1–8

[2] Ion A, Wall L, Kovacs R and Baudisch P 2017 Digital mechanical metamaterials *CHI Conf. on Human Factors in Computing Systems* pp 977–88

[3] Ren L, Wu W, Ren L, Song Z, Liu Q, Li B, Wu Q and Zhou X 2022 3D printing of auxetic metamaterials with high-temperature and programmable mechanical properties *Adv. Mater. Technol.* **7** 2101546

[4] Goh G L *et al* 2023 A 3D printing-enabled artificially innervated smart soft gripper with variable joint stiffness *Adv. Mater. Technol.* **8** 2301426

[5] Chen Y, Yan J and Feng J 2019 Geometric and kinematic analyses and novel characteristics of origami-inspired structures *Symmetry* **11** 1101

[6] Sato Y and Iwase E 2023 Self-folding method using a linkage mechanism for origami structures *Adv. Intell. Syst.* **5** 2200445

[7] Li M, Shen L, Jing L, Xu S, Zheng B, Lin X, Yang Y, Wang Z and Chen H 2019 Origami metawall: mechanically controlled absorption and deflection of light *Adv. Sci.* **6** 1901434

[8] Lazarus N, Bedair S S and Smith G L 2018 Origami inductors: rapid folding of 3-D coils on a laser cutter *IEEE Electron Device Lett.* **39** 1046–9

[9] Xu T, Zhang J, Salehizadeh M, Onaizah O and Diller E 2019 Millimeter-scale flexible robots with programmable three-dimensional magnetization and motions *Sci. Robot.* **4** eaav4494

[10] Li S, Stampfli J J, Xu H J, Malkin E, Diaz E V, Rus D and Wood R J 2019 A vacuum-driven origami 'magic-ball' soft gripper *IEEE Int. Conf. on Robotics and Automation (ICRA)* pp 7401–8

[11] Ryu J, Mohammadifar M, Tahernia M, Chun H-I, Gao Y and Choi S 2020 Paper robotics: self-folding, gripping and locomotion *Adv. Mater. Technol.* **5** 1901054

[12] Hong Y, Chi Y, Wu S, Li Y, Zhu Y and Yin J 2022 Boundary curvature guided programmable shape-morphing Kirigami sheets *Nat. Commun.* **13** 530

[13] Yasuda H, Johnson K, Arroyos V, Yamaguchi K, Raney J R and Yang J 2022 Leaf-like origami with bistability for self-adaptive grasping motions *Soft Robot.* **9** 938–47

[14] Wang H, Yang X, Qu H, Wang X, Liu W, Hu B and Guo S 2025 Construction and analysis of a thick-panel origami gripper with soft joints based on square-twist origami tessellation *Thin-Walled Struct.* **210** 113049

[15] Li H, Go G, Ko S Y, Park J-O and Park S 2016 Magnetic actuated pH-responsive hydrogel-based soft micro-robot for targeted drug delivery *Smart Mater. Struct.* **25** 027001

[16] Vlachaki E and Liapi K A 2021 Folded surface elements coupled with planar scissor linkages: a novel hybrid type of deployable structures *Curved Layered Struct.* **8** 137–46

[17] Na J-H, Evans A A, Bae J, Chiappelli M C, Santangelo C D, Lang R J, Hull T C and Hayward R C 2015 Programming reversibly self-folding origami with micropatterned photo-crosslinkable polymer trilayers *Adv. Mater.* **27** 79–85

[18] Miyashita S, Onal C D and Rus D 2013 Self-pop-up cylindrical structure by global heating *IEEE/RSJ Int. Conf. on Intelligent Robots and Systems* pp 4065–71

[19] Miyashita S, Guitron S, Li S and Rus D 2017 Robotic metamorphosis by origami exoskeletons *Sci. Robot.* **2** eaao4369

[20] Iwata Y, Miyashita S and Iwase E 2017 Self-rolling up micro 3D structures using temperature-responsive hydrogel sheet *J. Micromech. Microeng.* **27** 124003

[21] Liu Y, Shaw B, Dickey M D and Genzer J 2017 Sequential self-folding of polymer sheets *Sci. Adv.* **3** e1602417

[22] Zhang Q, Wommer J, O'Rourke C, Teitelman J, Tang Y, Robison J, Lin G and Yin J 2017 Origami and Kirigami inspired self-folding for programming three-dimensional shape shifting of polymer sheets with light *Extreme Mech. Lett.* **11** 111–20

[23] Cheng Y, Ren K, Yang D and Wei J 2018 Bilayer-type fluorescence hydrogels with intelligent response serve as temperature/pH driven soft actuators *Sens. Actuators B* **255** 3117–26

[24] Kim Y, Yuk H, Zhao R, Chester S A and Zhao X 2018 Printing ferromagnetic domains for untethered fast-transforming soft materials *Nature* **558** 274–9

[25] Lazarus N, Smith G L and Dickey M D 2019 Self-folding metal origami *Adv. Intell. Syst.* **1** 1900059

[26] Chung G, Chae J W, Han D-S, Won S M and Park Y 2024 Reprogrammable, recyclable origami robots controlled by magnetic fields *Adv. Intell. Syst.* **6** 2400082

[27] van Manen T, Janbaz S, Ganjian M and Zadpoor A A 2020 Kirigami-enabled self-folding origami *Mater. Today* **32** 59–67

[28] Ionov L 2011 Soft microorigami: self-folding polymer films *Soft Matter* **7** 6786–91

[29] Sung C, Lin R, Miyashita S, Yim S, Kim S and Rus D 2017 Self-folded soft robotic structures with controllable joints *IEEE Int. Conf. on Robotics and Automation (ICRA)* pp 580–7

[30] Eda A, Yasuga H, Sato T, Sato Y, Suto K, Tachi T and Iwase E 2022 Large curvature self-folding method of a thick metal layer for hinged origami/Kirigami stretchable electronic devices *Micromachines* **13** 907

[31] Hawkes E, An B, Benbernou N M, Tanaka H, Kim S, Demaine E D, Rus D and Wood R J 2010 Programmable matter by folding *Proc. Natl Acad. Sci.* **107** 12441–5

[32] Firouzeh A, Sun Y, Lee H and Paik J 2013 Sensor and actuator integrated low-profile robotic origami *IEEE/RSJ Int. Conf. on Intelligent Robots and Systems* pp 4937–44

[33] Boyvat M, Koh J-S and Wood R J 2017 Addressable wireless actuation for multijoint folding robots and devices *Sci. Robot.* **2** eaan1544

[34] Taylor A J, Slutzky T, Feuerman L, Ren H, Tokuda J, Nilsson K and Tse Z T H 2019 MR-conditional SMA-based origami joint *IEEE/ASME Trans. Mechatronics* **24** 883–8

[35] Liu J, Chen X, Lahondes Q, Esendag K, Damian D and Miyashita S 2022 Origami robot self-folding by magnetic induction *IEEE/RSJ Int. Conf. on Intelligent Robots and Systems (IROS)* pp 2519–25

[36] Liu W, Bai X, Yang H, Bao R and Liu J 2024 Tendon driven bistable origami flexible gripper for high-speed adaptive grasping *IEEE Robot. Autom. Lett.* **9** 2345–52

[37] Lahondes Q and Miyashita S 2024 Remotely actuated programmable self-folding origami strings using magnetic induction heating *Front. Robot. AI* **11** 1443379